The Journal of CPRI,
Vol. 4, No. 2, September 2008 pp. 135–147

Nanostructured Superhydrophobic Coatings

M Farzaneh* and D K Sarkar

A short description of the activities and facilities of the CIGELE/INGIVRE Chairs in relation with superhydrophobic and icephobic nanometric coatings has been reported. A brief description of how superhydrophobicity can help mitigate the ice accretion problem on power network equipment and other exposed structures by reducing adhesion of ice to surface has been presented. Basic models namely the Wenzel and Cassie-Baxter models accounting for the contact angle of water on solid surfaces relating to the influence of surface roughness on hydrophobicity have been discussed. The CIGELE/INGIVRE research team involved in the development of nanometric materials is actively working on the elaboration of superhydrophobic aluminium surfaces by chemical etching, superhydrophobic copper surfaces by silver nanoparticles, superhydrophobic nanostructured oxides and superhydrophobic nanofibres. Some of the promising results achieved on superhydrophobicity have been described.

Keywords: *Superhydrophobic, icephobic, chemical etching, plasma enhanced chemical vapour deposition, chemical bath deposition, sol-gel, electrospinning, nanotowers, silver nanoparticles, polymer nanofibres*

1.0 INTRODUCTION

The Industrial Chair on Atmospheric Icing of Power Network Equipment (CIGELE) was inaugurated in September 1997 with an initial mandate of five years (1997–2002). Its excellent performance led to the renewal of this mandate for a further period of five years (2002–2007). CIGELE is financed by a number of partner industries and organisations and benefits from grants of the Natural Sciences and Engineering Research Council (NSERC) of Canada and the Canada Foundation for Innovation (CFI).

CIGELE's mission is to study many of the phenomena associated with atmospheric icing, particularly the atmospheric icing of power network equipment, for the purpose of furthering knowledge in that area and disseminating the relevant research results. Part of its mission is also to train highly qualified personnel in this domain. For example, in the last ten years, more than 40 Masters and Ph.D. students were trained at CIGELE. The list of these trainees, as well as the publications they helped to produce can be found on the CIGELE website (www.cigele.ca).

On the eve of its renewal for a third five year mandate, CIGELE has extended its activities to include the development of nanostructured icephobic coatings for preventing the detrimental effects of ice accretion on power network equipment and other exposed structures.

Ice build-up on high tension power lines may lead to mechanical failure of the cables and to insulator flashovers, both entailing power outages and often severe costs. As a matter of

NSERC/Hydro-Québec/UQAC Industrial Chair on Atmospheric Icing of Power Network Equipment (CIGELE) and Canada Research Chair on Engineering of Power Network Atmospheric Icing (INGIVRE) at Université du Québec à Chicoutimi (UQAC), Canada. (www.cigele.ca)
* Corresponding author: Prof. M. Farzaneh, CIGELE/INGIVRE Chairholder, farzaneh@uqac.ca

fact, the ice storm that hit Eastern Canada in January 1998 caused several billions of dollars damage to the power networks and great hardship among the affected population.

In the past decades, researchers have tried to improve on the traditional, mechanical or chemical de-icing methods currently in use. Among these, freezing point depressants (salt, chemical sprays, etc.) for highways [1] and de-icing fluids (ethylene and propylene glycols) for aircraft [2] present drawbacks as to frequency of application, cost and toxicity. Other methods, specifically applicable to transmission lines like mechanical vibration of cables, Joule heating of the conductors [1] and electrolysis [3] are effective but consume lots of energy and necessitate surveillance of the lines and on-site intervention. None of these techniques prevents the formation or accumulation of ice. The prevention of ice formation on surfaces at sub-zero temperatures could be accomplished by producing coating materials that are icephobic in nature. Therefore, understanding the ice–solid interface should be considered an important aspect in achieving icephobic surfaces.

The strong adhesion of ice to materials is mainly a property of the ice–solid interface where polar ice molecules strongly interact with the solid. Among the three physical processes involved in ice adhesion namely, hydrogen bonding, van der Waals forces and direct electrostatic interactions, the latter has been found to be the dominant factor [4, 5]. In addition to the influence of electrostatic forces on ice adhesion, the morphology and composition of the solid surface plays an important role. Studies have been carried out to understand the role of surface roughness on ice adhesion using the concept of superhydrophobicity [6, 7].

1.1 Superhydrophobicity in nature

A surface exhibiting nearly zero wetting is said to be "superhydrophobic". Superhydrophobicity is observed on certain natural tissues. Among them, the surface of lotus leaves is the most obvious candidate for its inherent superhydrophobic and self-cleaning properties (Fig. 1A). The so-called "Lotus effect" is due to the presence of a rough micro-nanostructure (Fig. 1B) covered with waxy materials which are poorly wetting, resulting in a water contact angle slightly above 150° [8]. The rough structure allows a large amount of air entrapment in between the gaps of the micro/nanostructure resulting in a heterogeneous surface composite, where air and the waxy tissue provide a very low surface energy enhancing the contact angle of the rough structure. Learning from nature, a superhydrophobic surface can be obtained by creating a surface of optimum roughness followed by passivation with a low surface energy coating. As the contact area of water on a superhydrophobic solid surface is negligible, it would effectively reduce the contact area of ice. Therefore, ice adhesion would be significantly reduced on superhydrophobic surfaces.

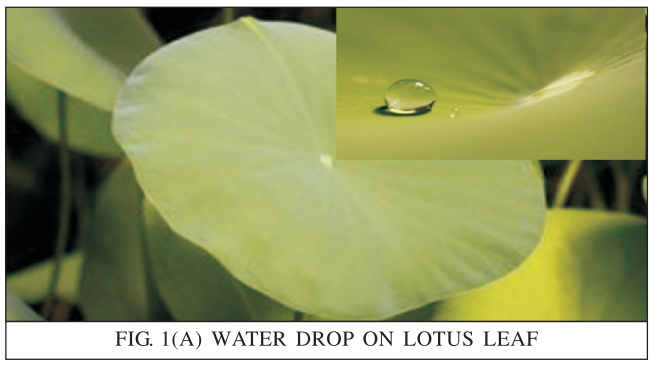

FIG. 1(A) WATER DROP ON LOTUS LEAF

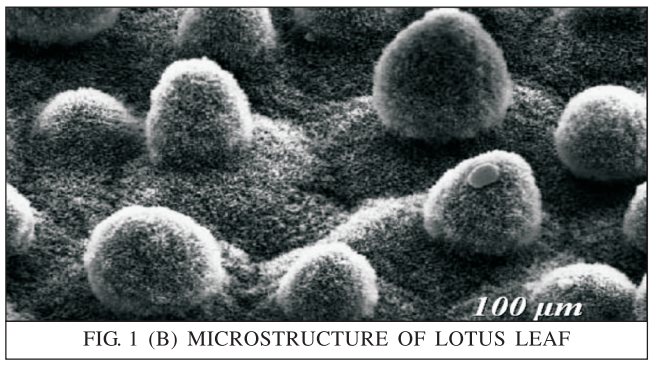

FIG. 1 (B) MICROSTRUCTURE OF LOTUS LEAF

1.2 Classical models governing wettability

A very basic and commonly used relation Equation (1) describing wettability with respect to the contact angle of a drop in equilibrium with a solid surface was given by Young [9]. It relates the interfacial free energies of the three interfaces the drop comes in contact with, when placed on a solid surface, namely the solid/liquid (γ_{SL}), solid/vapour (γ_{SV}), and liquid/vapour (γ_{LV}) interfaces. The line of contact

with the three co-existing phases of the system makes an angle of contact, θ , with the surface.

$$\cos\theta = \frac{\gamma_{SV} - \gamma_{SL}}{\gamma_{LV}} \quad (1)$$

To reach contact angle values greater than 150°, necessary for achieving superhydrophobicity, surface roughness is often added to enhance the hydrophobicity of the solid surface. The surface topography effects have been mathematically expressed by the Wenzel and the Cassie-Baxter equations [10, 11]. The Wenzel equation is expressed as

$$\cos\theta' = R_w \cos\theta \quad (2)$$

where the roughness factor R_w is the ratio of the true to the apparent surface areas.

The Cassie-Baxter model, however, describes the effect of roughness on chemically heterogeneous structures where the apparent contact angle is mathematically derived from the Cassie equation as follows:

$$\cos\theta' = f_1 \cos\theta_1 + f_2 \cos\theta_2 \quad (3)$$

where θ' is the contact angle of the composite coating consisting of two components with contact angles θ_1 and θ_2, and their corresponding area fractions f_1 and f_2. In such a composite system, f_1 is assumed to be the area fraction of the solid surface, f_2 is assumed to be that of air, where θ_2 is 180°. As $f_1 + f_2 = 1$, Equation (1) can be further modified as

$$\cos\theta' = f_1(\cos\theta_1 + 1) - 1 \quad (4)$$

This equation explains why, on a rough surface with a large amount of air entrapment in the surface irregularities, one can obtain a highly super-hydrophobic surface with a very small area fraction f_1 of the surface in contact with the water drop.

1.3 Nanotechnology's contribution in the engineering of superhydrophobic surfaces

Nanotechnology presents paramount advantages. It facilitates the integration and miniaturisation of devices, resulting in a variety of scientific developments including environmental safety and energy consumption, miniaturisation and many others [12-21]. Wettability is a fundamental property of solid surfaces which plays an important role in daily life and several industrial applications [22]. On the other hand, various phenomena such as contamination, snow accretion and erosion are expected to be inhibited on superhydrophobic surfaces [23]. Superhydrophobic nanostructured surfaces may also play an important role in reducing adhesion of snow and ice to surfaces [7] carrying along with anti-corrosive effects, which may lead to important applications such as coatings for cables, insulators, aircraft wings, ship hulls, glass windows and car windshields. The two basic essential factors associated with achieving superhydrophobic properties on a surface are an optimised surface roughness and low surface energy. Inspired by surface engineering found in nature, and using the concepts provided by the Wenzel and Cassie–Baxter models, the ways for preparing superhydrophobic surfaces can be generally categorised into the top-down and bottom-up approaches.

Top-down approaches encompass lithographic and template-based techniques [24], micromachining [6], and plasma treatment of the surfaces [25, 26]. Bottom-up approaches involve mostly self-assembly and self-organisation [27] such as chemical bath deposition (CBD) [28, 29], chemical vapour deposition (CVD) [30], and electrochemical deposition [31]. Techniques involving combination of both approaches, such as casting of polymer solution, phase separation [32] and electrospinning [33, 34] are also being commonly used.

The research activities carried out at CIGELE are unique as compared to those of several other research groups also working in the field of superhydrophobicity due to the fact that its facilities allow not only superhydrophobicity tests, but also ice adhesion tests on surfaces.

2.0 INFRASTRUCTURES AT CIGELE ON NANOMETRIC RESEARCH

The CIGELE laboratories are equipped with very sophisticated instruments for the preparation and

characterisation of nanostructured materials. The equipment used for materials research is described in this section. Apart from the materials research, it includes several cold chambers to produce atmospheric ice, mechanical test systems (MTS) to measure ice adhesion on solid surfaces, bending strength and stress of atmospheric ice, and to perform several other ice adhesion tests, refer CIGELE website (www.cigele.ca) for further information.

2.1 Instruments/techniques for the synthesis of materials

2.1.1 Micro-emulsion process

In this process, metallic nanoparticles are prepared from metallic salts in an alcoholic medium which acts both as a solvent and a reducing agent of metallic ions.

For the preparation of silver nanoparticles, for example, a certain volume of monoethylene glycol (EG) is heated to reach 160°C under vigorous stirring in a round-bottom three-necked flask as shown in Fig. 2.

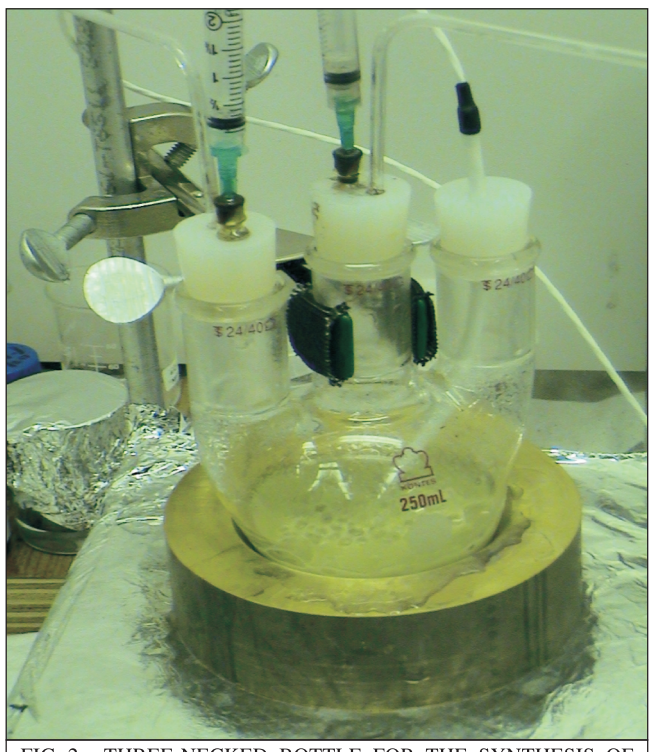

FIG. 2 THREE-NECKED BOTTLE FOR THE SYNTHESIS OF METALLIC NANOPARTICLES BY CHEMICAL ROUTES

Solutions of $AgNO_3$ and poly-vinylpirrolidone (PVP) both in EG are then prepared and simultaneously injected into the flask followed by continuous stirring.

2.1.2 Sol-gel technique

The sol-gel process involves the evolution of inorganic networks through the formation of a colloidal suspension (sol) and the gelation of the sol to form a network in a continuous liquid phase (gel) [35]. Two instruments namely the spin-coater and the dip-coater are used for the purpose of coating the films using sol-gel techniques.

A spin-coater is used for precise and uniform deposition of thin film coatings. A typical process involves depositing a small volume of a sol onto the center of a substrate and then spinning the substrate at high speed. The spin-coater used at CIGELE (Fig. 3A) is a natural polypropylene portable tabletop model with a 8.5" diameter bowl-shaped process chamber that can accommodate upto 6" diameter or 4" ×4" square substrates.

On the other hand, dip coating involves immersing of a substrate into a beaker containing coating material in solution form, removing the piece from the beaker with a very slow speed (10-100 μm/s), and allowing it to dry by heating. CIGELE's home made dip-coater (Fig. 3B) is fully computer-controlled and designed for single layer coating.

FIG. 3(A) SPIN-COATER

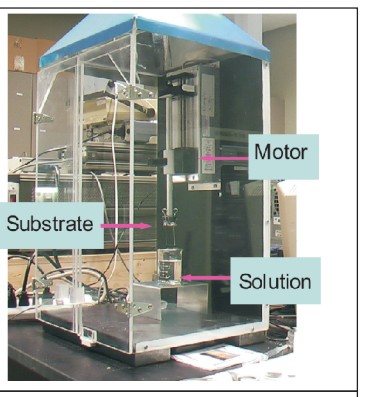

FIG. 3(B) DIP-COATER

2.1.3 Plasma reactor (PECVD/PVD)

Apart from thin film deposition using chemical processes, CIGELE is also equipped with a plasma reactor that allows plasma enhanced chemical vapour deposition (PECVD) and physical vapour deposition (PVD). In the PECVD process, hard films of diamond-like carbon (DLC) are routinely prepared using discharge of CH_4 and Ar gas using rf-source. In addition, low surface energy hard coating of fluorinated DLC (F-DLC) is produced by incorporating fluorine using C_2F_6 gas during DLC coating. In the PVD process, a Teflon target is sputtered to produce thin films of Teflon on nanostructured surfaces to obtain low surface energy superhydrophobic coatings.

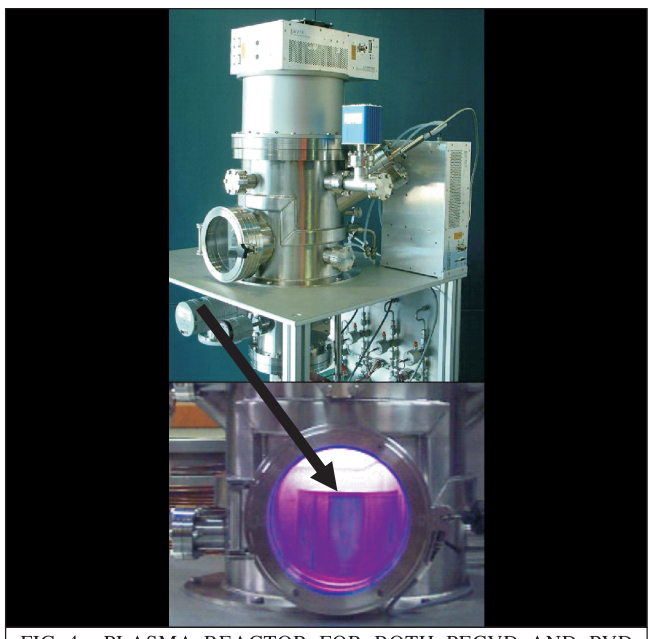

FIG. 4 PLASMA REACTOR FOR BOTH PECVD AND PVD COATING

2.2 Instruments/techniques for the characterisation of materials

2.2.1 Atomic force microscope (AFM)

The EnviroScope atomic force microscope (Fig. 5) combines modular environmental controls, a sealed hermetic sample chamber, and a wide range of imaging modes to bring superior application flexibility to research and industrial facilities. The system allows the observation of sample reactions in a variety of complex environmental changes. The EnviroScope's scanner includes a piezoelectric tube scanner, a laser, and a quadrature optical detector capable of delivering proven scanning probe performance and reliability. The microscope is capable of imaging sub-zero and below –10°C samples, and is suitable for the study of ice/matter interactions.

FIG. 5 AFM: ENVIROSCOPE PROVIDED BY VEECO

2.2.2 Drop analyser: Contact angle measurement tool

The Drop Shape Analysis System DSA100 provided by Krüss GmbH (Fig. 6) is an ideal tool to measure contact angle of a drop of liquid on a surface as well as the contact angle hysteresis. The unique adjustment of the observation angle allows one to see the drop, permitting adjustment of the dosing systems without the risk of contaminating the sample.

FIG. 6 DROP ANALYSER FOR MEASURING CONTACT ANGLE AND HENCE SURFACE ENERGY

This system can be used for the determination of surface treatments, examination of adhesive properties, surface purity check and optimisation of a broad variety of coatings. An additional special stage has been attached that can bring the sample surface temperature below –20°C and make this system suitable for contact angle measurements below 0°C.

3.0 STUDY OF NANOSTRUCTURED SUPERHYDROPHOBIC COATING IN CIGELE

Substantial progress has been made in the last years in this research at CIGELE [29, 33, 36-44]. In this section, we will present an overview of the current CIGELE projects in nanometric research.

3.1 Superhydrophobic properties of aluminum surfaces

Rolled sheets of aluminium alloy (AA6061) of dimension 25 mm × 25 mm × 1.58 mm were used as substrates. The substrates were etched with 14.8 wt.% hydrochloric acid (HCl) for different times ranging from 1 to 5 minutes. The etched clean samples were dried and further coated with ultrathin Teflon films by rf-sputtering using Ar plasma in an inductively coupled plasma reactor.

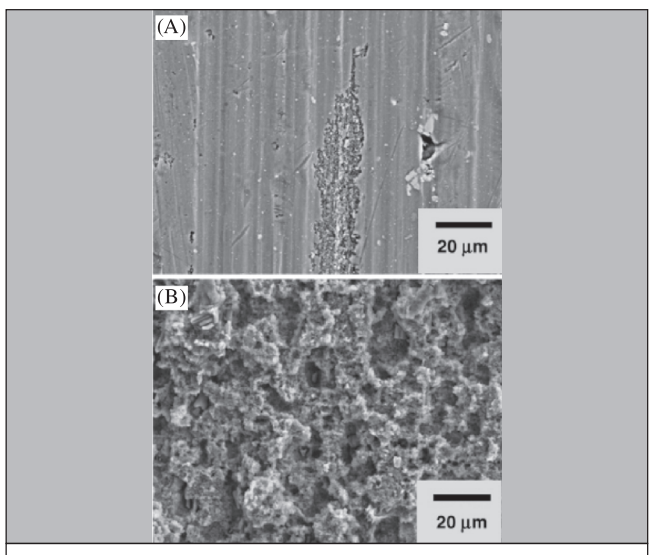

FIG. 7 FESEM IMAGES OF rf-SPUTTERED TEFLON COATED (A) AS RECEIVED ALUMINUM SUBSTRATE (B) ALUMINUM SUBSTRATES ETCHED WITH 14.8 wt% HCl FOR 2.5 MINUTES

Fig. 7 shows FESEM images of rf-sputtered Teflon coated (A) as-received aluminum substrate (B) aluminum substrates etched with 14.8 wt% HCl for 2.5 minutes. It is clear from Fig. 7 (B) that etch pits are formed on the aluminum surface after etching with HCl acid which effectively change the surface morphology [45, 46].

X-ray photoelectron spectroscopy (XPS) analysis confirms the presence and the chemical composition of the rf-sputtered Teflon films. Fig. 8 shows the C 1s peak of a rf-sputtered Teflon film. Fig. 9A shows the change in thickness of the aluminum substrates with etching time. The thickness of the as-received aluminum substrates is 1.58±0.006 mm. However, after 2.5 minutes of etching period, the thickness is reduced to 1.46±0.014 mm, and then further reduced to 1.25±0.012 mm after prolonging the etching period to 5 minutes.

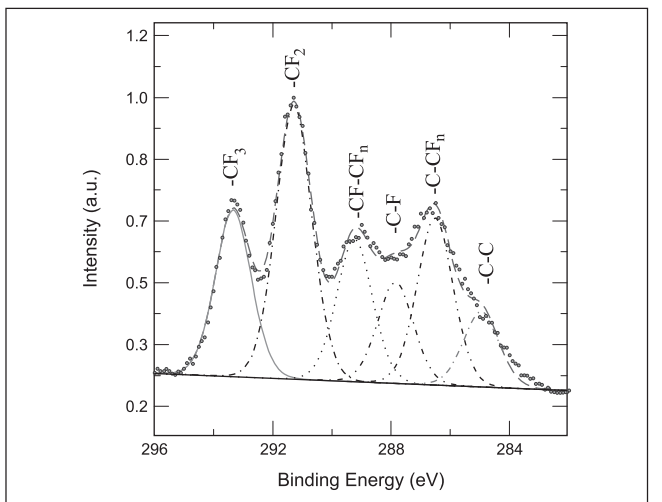

FIG. 8 X-RAY PHOTOELECTRON SPECTROSCOPY (XPS) SPECTRUM OF C 1s OF rf-SPUTTERED TEFLON FILMS

The change in thickness of the aluminum substrates etched between 2 and 5 minutes of duration follows a first order exponential decay law with time as presented in Equation (5):

$$d = 1.22 + 1.74\exp(-t/1.28) \quad (5)$$

where d is the thickness of the aluminum substrates and t is the time of etching. Fig. 9B shows the contact angle data of water on rf-sputtered Teflon thin film coated etched aluminum substrates.

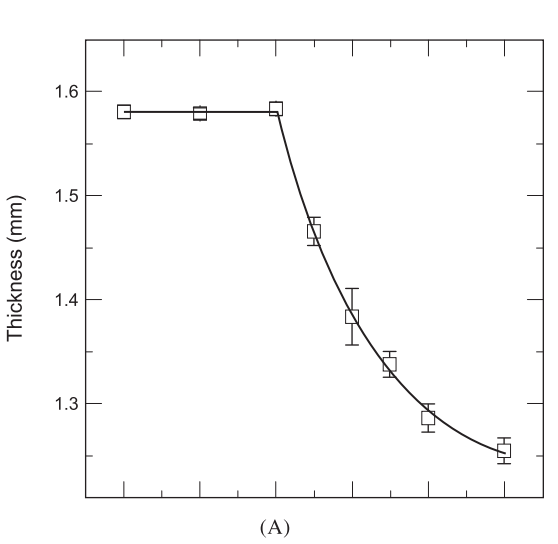

(A)

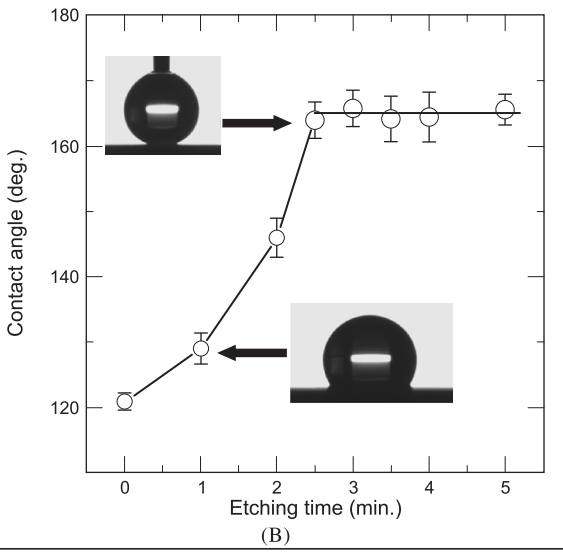

(B)

FIG. 9 (A) CHANGE OF THICKNESS OF ALUMINUM SUBSTRATES WITH ETCHING TIME (B) CONTACT ANGLE OF WATER

rf-sputtered Teflon coated as received aluminum substrate showed a contact angle of ~121±1.3°. The contact angle increased to 164±3° for the aluminum substrates that were etched for 2.5 minutes.

It is interesting to note that the contact angle remains constant on the aluminum surfaces that were further etched for longer than 2.5 minutes as shown in Figure 9B. An average contact angle hysteresis of 2.5±1.5° has been achieved on Teflon-coated etched aluminum surfaces. The contact angle values similar to our observation or even higher have been reported in recent literature [28]. An average contact angle hysteresis of 2.5±1.5° has been achieved on Teflon coated etched aluminum surfaces. The insets of Fig. 9B show the shapes of a water drop on 1 minute and 2.5 minutes etch surfaces for visualising the values of contact angles.

The existence of a large number of CF_3 groups along with CF_2 groups makes the etched aluminum surfaces highly superhydrophobic, providing a water contact angle of ~ 164±3° with a very low contact angle hysteresis, lesser than 2.5±1.5°. Water drops simply roll off from such surfaces. This simple, low cost and efficient way of preparing substrates with superhydrophobic properties have promising industrial applications.

3.2 Superhydrophobic properties of silver nanoparticles coated copper surfaces

Ultrasonically cleaned copper substrates have been coated with silver thin films by immersing in a silver nitrate solution which involves a chemical reaction in which copper reduces silver ions spontaneously as described by the following equation.

$$2Ag^{+} + Cu \rightarrow 2Ag + Cu^{2+} \quad (6)$$

After drying, the silver coated samples were passivated with stearic acid organic molecules dissolved in acetone. Figs. 10A, B and C show SEM images of samples prepared in three different initial Ag^+ concentrations of 13.2, 24.75 and 396 mM, respectively in the solution. It can be seen that the size and number of both the fractal-like structures and voids surrounded by them are concentration dependent. Due to the low Ag^+ ion concentration in the solution, the reaction is slow and the film has tiny, almost indistinguishable voids, as shown in Fig. 10A. After stearic acid passivation, this sample shows a water contact angle and a contact angle hysteresis of 137° and 27° respectively, as shown in the inset of Fig. 10A. When the initial Ag^+ ions concentration increases in the solution, the reaction becomes rapid and larger fractal-like structures of silver appear.

Consequently, the size of the voids between these structures also increases. The average diameter of the voids is ~5 μm as shown in Fig. 10B. The contact angle and the contact angle hysteresis obtained are 156° and 4° respectively as shown in the inset of Fig. 10B. By further increasing the concentration of Ag^+ ions in the solution, the size of the voids increases to ~10 μm, as seen in Fig. 10C, with a contact angle and hysteresis of 141° and 16° respectively as shown in the inset of Fig. 10C. The highest contact angle and the lowest contact angle hysteresis were achieved for the sample having void sizes of ~5μm, obtained with initial silver ions concentration of 24.75 mM in the solution. Fig. 10D shows a magnified fractal-like structure from Fig. 10B.

It was observed that apart from voids between the fractal-like structures, there are several empty spaces between them due to its self-similar structure.

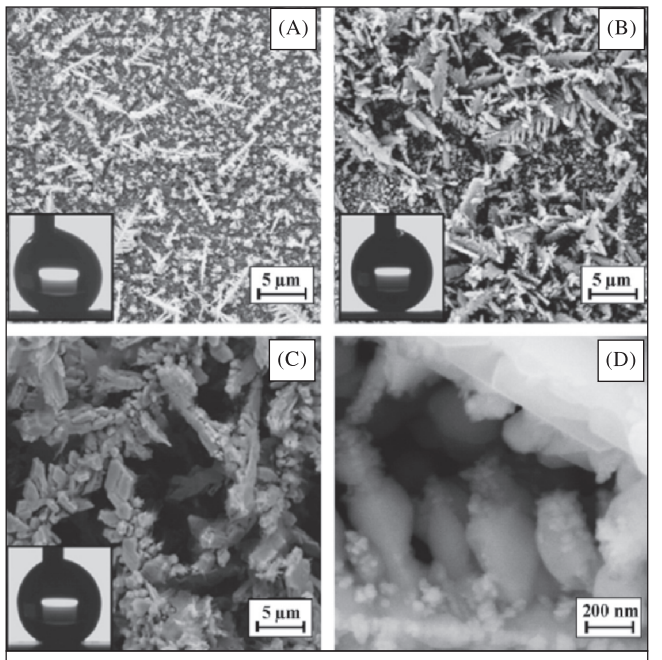

FIG. 10 SEM IMAGES OF SAMPLES PREPARED IN THREE DIFFERENT INITIAL Ag^+ CONCENTRATIONS OF (A) 13.2 mM, (B) 24.75 mM (C) 396 mM RESPECTIVELY; AND (D) A MAGNIFIED SECTION OF (B).

3.3 Superhydrophobic properties of nanostructured ZnO thin films

ZnO nanotowers were grown on ultrasonically cleaned silicon substrates by means of the chemical bath deposition technique (CBD), and then dried for several hours [29]. The as-prepared ZnO samples were then passivated with 2 mM stearic acid (SA) in acetone for 30 minutes by immersion. Another set of sol-gel ZnO thin films spin-coated by using 0.02 M methanolic zinc acetate and annealing at 450°C after drying at 120°C on a hot plate were also passivated with 2 mM SA molecules using a similar method as that of CBD films. The passivated CBD grown samples were annealed in air for 30 minutes at different temperatures ranging from 70°C to 350°C for thermal desorption studies.

The growth process of ZnO nanotowers involves a chemical reaction during which the zinc nitrate decomposes to release ZnO in the presence of ammonium hydroxide [29].

Fig. 11 shows the field emission scanning electron microscopy (FESEM) images of the ZnO nanotowers while Fig. 11A shows the presence of randomly oriented hexagonal patterned ZnO nanotowers, characterised by regular edges with an angle of 120° between the adjacent sides, as shown in Figs. 11B and 11C. The top few nanometers of each nanotower consist of uniform nanosteps revealing the presence of a rough binary structure.

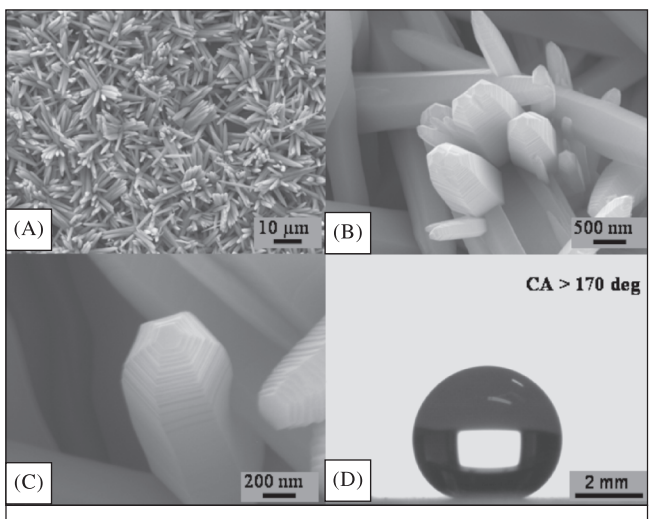

FIG. 11 FESEM IMAGES OF ZnO NANOTOWERS AT (A) LOW MAGNIFICATION (B) HIGH MAGNIFICATION SHOWING THE HEXAGONAL MORPHOLOGY (C) CLOSE-UP VIEW OF A SINGLE NANOTOWER SHOWING THE NANOSTEPS (D) IMAGE OF A WATER DROP FOLLOWING SA PASSIVATION.

After passivation with SA, these ZnO nanotowers become highly superhydrophobic, providing a contact angle as high as ~173° and a contact angle hysteresis as low as ~1.5°. However, SA passivated smooth ZnO coating prepared by spin-coating provides a contact angle of ~73.5 ± 4°, as shown in the inset of the AFM image of Fig. 12.

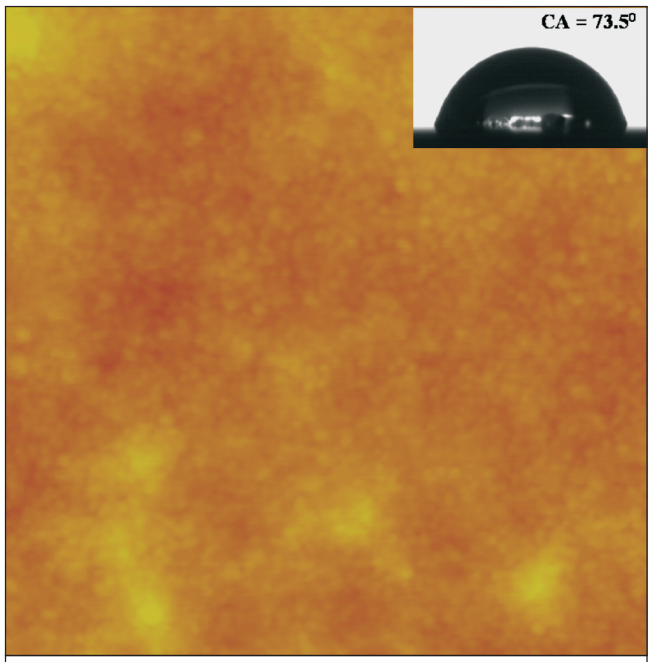

FIG. 12 AFM IMAGE OF SPIN-COATED ZnO THIN FILM WITH AN IMAGE SCAN SIZE 1 µm × 1 µm. INSET SHOWS THE IMAGE OF A WATER DROP ON THIS SURFACE

To the best of our knowledge, no such results on contact angle of water on stearic acid passivated smooth ZnO surface were reported in the literature. The smooth and dense sol-gel derived spin-coated ZnO thin film is composed of scattered ~20 nm tiny ZnO particles with an *rms* roughness of ~2 nm. The obtained contact angle results are consistent with previous observations on stearic acid impregnated with cellulose surface [47]. The fraction of solid surface (f_1) is calculated using the modified Cassie equation (Equation (4)) for SA passivated ZnO nanotowers (composite of SA/ZnO and air) with θ_1 and θ_2 values of 73° and 173° respectively. The calculated f_1 factor is ~0.006. Such a small value of f_1 confirms the existence of trapped air between the nanotowers. Fig. 11D shows the image of a water drop captured on the surface of these ZnO nanotowers after SA passivation.

A Fourier transform infrared (FTIR) spectra of the SA modified ZnO nanotowers confirms the presence of the -CH_n groups of SA. Fig. 13 shows the FTIR spectra of the samples, annealed at different temperatures, in the wave number range of 2550-3150 cm^{-1} showing only the -CH_n peaks of stearic acid. The two peaks at wave numbers 2919 cm^{-1} and 2850 cm^{-1} belong to the asymmetric and symmetric C-H stretching modes of $-CH_2$, the groups of stearic acid respectively, and the peak at 2958 cm^{-1} is ascribed to the asymmetric in-plane C-H stretching mode of the -CH_3 group [48].

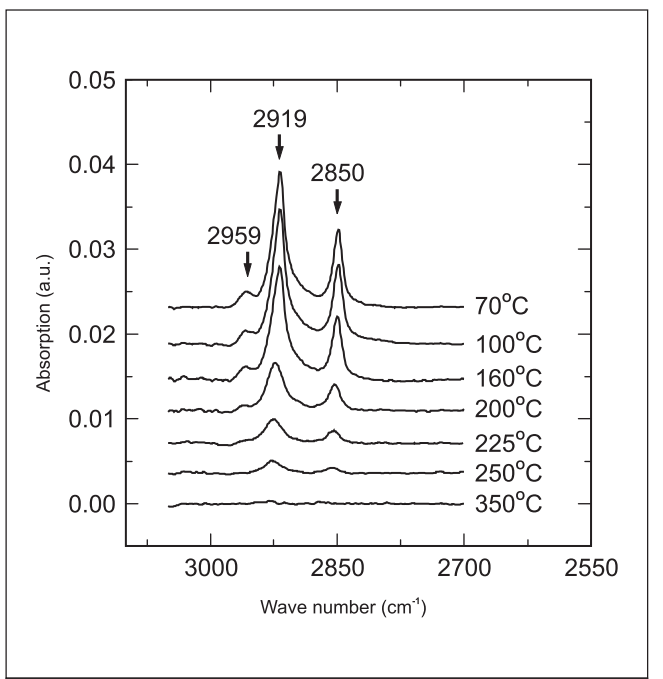

FIG. 13 FTIR SPECTRA SHOWING -CH_n PEAKS OF STEARIC ACID FOLLOWING ANNEALING AT VARIOUS TEMPERATURES

The three peaks of stearic acid remain nearly unchanged until 160°C with a drastic change occurring in their intensity at 200°C due to thermal desorption and a continued decrease in intensity with increasing temperature. Fig. 14 shows the contact angle and contact angle hysteresis data following annealing at elevated temperatures. The contact angle, as shown in the inset of Fig. 14 remains higher than 170° upto 160 °C, and then starts dropping with a minor decrease upto 250 °C, at which point the contact angle is greater than 160°, still showing superhydrophobicity.

The contact angle hysteresis (Fig. 14) undergoes an increase with increasing annealing temperature, from 1.5° at 70°C to 6° at 250°C, although water drops still keep rolling off the surface easily. However, the contact angle continues to fall with increasing annealing temperature.

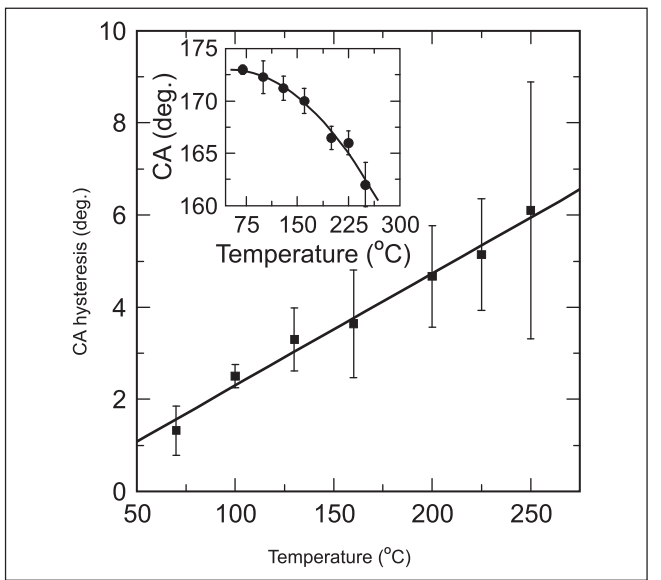

FIG. 14 CONTACT ANGLE HYSTERESIS VERSUS TEMPERATURE INSET SHOWS CONTACT ANGLE VERSUS TEMPERATURE

A strong correlation has been established between the thermal desorption of stearic acid and the superhydrophobic behaviour of ZnO nanotowers. Fig. 13 shows a nearly constant contact angle with a very low contact angle hysteresis at room temperature, following annealing at 160°C. This is due to the presence of nearly constant stearic acid peak intensity until the annealing temperature of 160°C as observed in Fig. 13. As the density of the stearic acid starts to decrease after an annealing temperature of 160°C, the contact angle begins to decrease, with an increase, although not great, in contact angle hysteresis.

Following annealing at 350°C, the water drop spreads completely on the surface and the FTIR spectra show a zero intensity of the -CH_n peaks. Due to complete desorption of SA at 350°C, the water drop directly interacts with ZnO, showing hydrophilic behaviour of the ZnO surface. The thermal desorption of stearic acid is found to occur at approximately 184 °C with an activation energy of 0.34 ± 0.05 eV.

3.4 Superhydrophobic polymer nanofibres

Nanofibres of polymers (polystyrene) of diameter around 500nm and 2μm, for low and high viscous polymer solutions, respectively, have been created by electrospinning, as presented in Fig. 15 [33]. Highly viscous solutions produced ribbon-like structures, whereas less viscous ones produced agglomerated polymer nanofibres connected with narrow fibres.

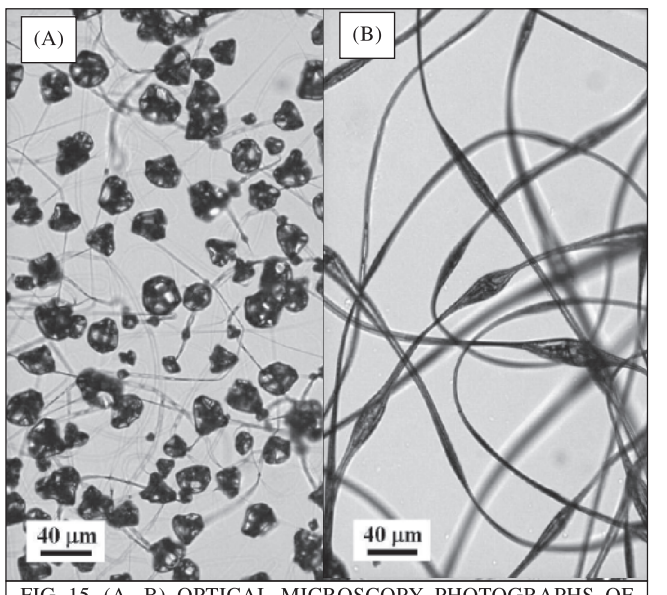

FIG. 15 (A, B) OPTICAL MICROSCOPY PHOTOGRAPHS OF ELECTROSPUN PS MATS OBTAINED FROM LIQUID SOLUTIONS. *U* = 20 kV AND *F*r = 1 mL h^{-1}. *C*PS = 14 % (A) AND 18 % w/w (B).

These polymer nanofibres do not show superhydrophobicity. To obtain superhydrophobicity, however, PTFE particles were suspended in the PTVFP polymer solution and electronspun on solid surfaces. High-viscosity solutions yielded a fibre structure, as shown in Fig. 16A, while the low-viscosity solutions yielded a fibre-bead-like structure with beads having an ellipsoidal shape (Fig. 16B).

It is important to notice that the fibre structure presented in Fig. 16A has closed porosity while open porosity occurrences are scarce (see areas 1 and 2 of Fig. 16A). Additionally, independent of the applied voltage, increasing solution flow rates led to an increase in fibre diameters reaching as high as 9 μm.

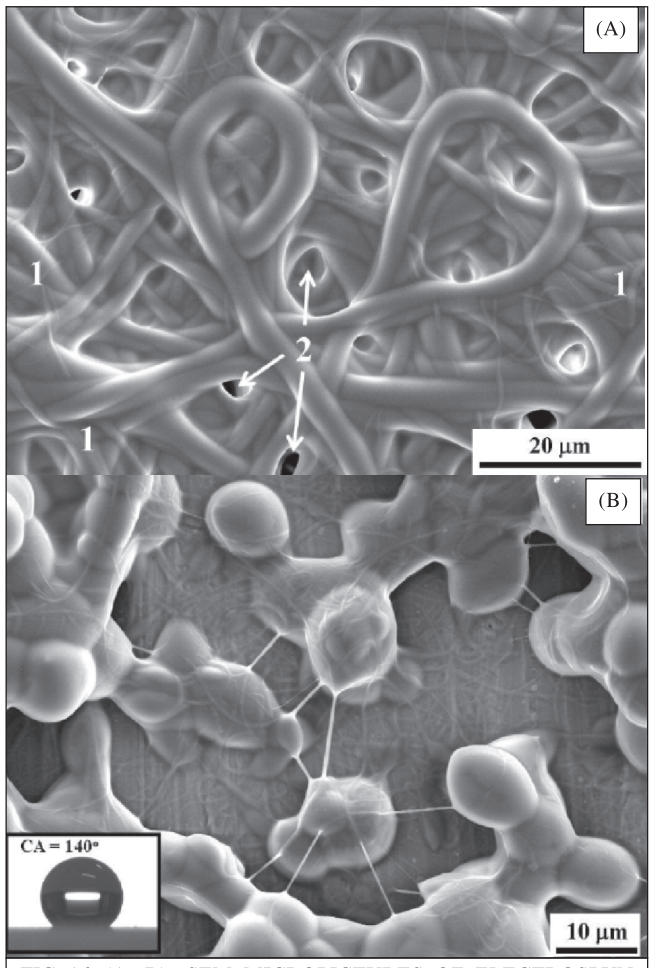

FIG. 16 (A, B): SEM MICROPICTURES OF ELECTROSPUN PTVFP MATS OBTAINED FROM LIQUID SOLUTIONS. U = 25 kV AND Fr = 1 mL h^{-1}. ·= 2062 (A) AND 67 MPA S (B).

As regards the low-viscosity solutions, the corresponding mats were made of ellipsoidal beads with their minor ($d1$) and major axis ($d2$) lengths comprising between 9.3 and 12.6 μm and between 10.6 and 15.4 μm respectively.

4.0 INFLUENCE OF SUPERHYDROPHOBICITY IN ANTI-ICING APPLICATIONS

It has been observed that fluorinated and polysiloxane modified surfaces show the poorest wetting by water and the best potential as icephobic coatings [49]. Studies have also shown that aluminum surfaces rendered hydrophobic, by the addition of a self-assembled monolayer (SAM) of silane and fluorocarbon, have reduced the ice adhesion compared to bare aluminum surfaces [50, 51]. It has been also reported that snow accumulation on nanostructured superhydrophobic surfaces is reduced as compared to smooth surfaces [6, 7].

5.0 CONCLUSIONS

A new domain of research has been initiated at CIGELE on the development of icephobic nanometric coatings in order to provide working and economic solutions to the age-old problem of ice accretion on structures and its detrimental effects, particularly on power network equipment. Based on patterns found on superhydrophobic surfaces found in nature, and using the Wenzel and Cassie-Baxter models to explain the behaviour of water drops on solid surfaces and the effect of surface roughness on the enhancement of contact angle, several interesting results have been achieved on superhydrophobicity of metals, oxides and polymers. For example, superhydrophobic micro-patterned aluminum surfaces have been created by chemical etching using hydrochloric acid. A water contact angle as high as 164±3° with a contact angle hysteresis as low as 2.5±1.5° have been achieved on rf-sputtered Teflon coated etched aluminum substrates. Also, a simple process was developed to produce stable superhydrophobic surfaces with contact angles as high as ~156° and contact angle hysteresis as low as ~4° by the combination of the galvanic ion exchange reaction between silver ions with copper surface and passivation with stearic acid organic molecules. As far as the superhydrophobic oxide nanostructure is concerned, it was demonstrated that stearic acid passivated ZnO nanotowers, with a binary structure composed of several nanosteps on each nanotower, have a very high contact angle of ~173° with a very low contact angle hysteresis of ~1.5°.

The superhydrophobicity deteriorates with increasing annealing temperature due to the thermal desorption of stearic acid that occurs at approximately 184°C with an activation energy of 0.34 ± 0.05 eV. Production of superhydrophobic polymeric nanofibres was also achieved.

6.0 ACKNOWLEDGMENTS

This study was carried out within the framework of the NSERC/Hydro-Québec/UQAC Industrial Chair on Atmospheric Icing of Power Network Equipment (CIGELE), as well as the Canada Research Chair on the Engineering of Power Network Atmospheric Icing (INGIVRE). The authors would like to thank all the sponsors for their financial support and are grateful to Dr R Menini, senior researcher, N Saleema and A Safaee, Ph.D. students, for their involvement in some tests and useful discussion.

REFERENCES

[1] "Minimizing Effects from Highway Deicing", EPA 832-F-99-016, 1999.

[2] "Airplane Deicing Fluid Recovery Systems", EPA 832-F-99-043, 1999.

[3] Petrenko V F and S Qi, J. Appl. Phys. 86, 5450, 1999.

[4] Ryzhkin I A, and Petrenko V F, J. Phys. Chem. B, 101, 6267, 1997.

[5] Petrenko V F and Whitworth R W, "Physics of Ice", Oxford University Press, Oxford, 1999.

[6] Laforte C, J. -L. Laforte, and Carrier J C, "Proceedings of the International Workshop on Atmospheric Icing of Structures (IWAIS)", 6 p., 2002.

[7] Saito H, Takai K, and Yamauchi G, Surf. Coat. Int., 80, 4, 1997.

[8] Barthlott W, and Neinhuis C, Planta, 202, 1, 1997.

[9] Young T, Phil. Trans. R. Soc. Lond. 95, 65, 1805.

[10] Wenzel R N, Ind. Eng. Chem., 28, 988, 1936.

[11] Cassie A B D, Baxter S, Trans. Faraday Soc. 40, 546, 1944.

[12] Sarkar D K, Brassard D and El Khakani M A, Appl. Phys. Lett 87, 253180, 2005.

[13] Sarkar D K, Cloutier F and El Khakani M A, J. Appl. Phys. 97, 084302, 2005.

[14] Sarkar D K, Brassard D, El Khakani M A, and Ouellet L, Thin Solid Films 515, 4788, 2007.

[15] Brassard D, Sarkar D K, El Khakani M A, and Ouellet L, "Journal of Vacuum Science Technology A: Vacuum, Surfaces, and Films" 24, 600, 2006.

[16] Brassard D, Sarkar D K, El Khakani M A, Ouellet L, J. Vac. Sci. Technol. A 22, 851, 2004.

[17] Sarkar D K, Zhou X J, Tannous A, Louie M, Leung K T, "Solid State Communications" 125, 365, 2003.

[18] Sarkar D K, Zhou X J, Tannous A, Leung K T, J. Chem. Phys. B (Letter) 107, 2879, 2003.

[19] Sarkar D K, Desbiens E, El Khakani M A, Appl. Phys. Lett 80, 294, 2002.

[20] Sarkar D K, Rau I, Falke M, Giesler H, Teichert S, Beddies G and H. -J. Hinneberg, Appl. Phys. Lett. 78, 3604–3606, 2001.

[21] Sarkar D K, Falke M, Giesler H, Teichert S, Beddies G and H. -J. Hinneberg, J. Appl. Phys. 89, 6506–6513, 2001.

[22] Sun T, Feng L, Gao X, Jiang L, Acc. Chem. Res. 38, 644, 2005.

[23] Lafuma A, Quéré, Nature Mater D. 2, 457, 2003.

[24] Li J, Fu J, Cong Y, Wu Y, Xue L J, Han Y C, Appl. Surf. Sci. 252 (2006) 2229.

[25] Stelmashuk V, Biederman H, Slavinska D, Zemek J, Trchova M, Vacuum 77, 131, 2005.

[26] Kim S H, Kim J H, Kang B K, Uhm H S, Langmuir 21, 12213, 2005.

[27] Schondelmaier D, Cramm S, Klingeler R, Morenzin J, Zilkens C, Eberhardt W, Langmuir 18, 6242, 2002.

[28] Honoso E, Fujihara S, Honma I, Zhou H, J. Am. Chem. Soc. 127, 13458, 2005.

[29] Saleema N, Sarkar D K, Farzaneh M, Sacher E, "Proceedings of the 2006 NSTI Nanotechnology Conference and Trade Show", Boston, Massachusetts, USA, Vol. 3, pp. 158, May 2006.

[30] Liu H, Feng L, Zhai J, Jiang L, Zhu D B, Langmuir 20, 5659, 2004.

[31] Shi F, Wang Z Q, Zhang X, Adv. Mater. 17, 1005, 2005.

[32] Jiang L, Zhao Y, Zhai J, Angew. Chem. Int. Ed. 43, 4338, 2004.

[33] Menini R and Farzaneh M, Polymer International (in press 2007).

[34] Acatay K, Simsek E, Ow-Yang C, Menceloglu Y Z, Angew. Chem. Int. Ed. 43, 5210, 2004.

[35] Lev O, Tsionsky M, Rabinovich L, Glezer V, Sampath S, Pancratov I, Gun J Anal. Chem. 67, 22A, 1995.

[36] Kulinich S A, Farzaneh M, DU X W, "Inorganic Materials" (in press 2007).

[37] Kulinich S A and Farzaneh M, Vacuum 79, 255, 2005.

[38] Kulinich S A and Farzaneh M, Surf. Sci. 573, 379, 2004.

[39] Kulinich S A and Farzaneh M, Appl. Surf. Sci. 230, 232, 2004.

[40] Sarkar D K and Farzaneh M, "Proceedings of the 2006 MST Conferences, Fifth International Symposium on Contact Angle Wettability and Adhesion", Toronto, Canada, Session IV, June 2006.

[41] Saleema N, Sarkar D K, Farzaneh M, Proceedings of the 2006 MST Conferences, "Fifth International Symposium on Contact Angle Wettability and Adhesion", Toronto, Canada, Session IV, June 2006.

[42] Safaee A, Sarkar D K, Farzaneh M, "Proceedings of the 2006 MST Conferences, Fifth International Symposium on Contact Angle, Wettability and Adhesion", Toronto, Canada, Session IV, June 2006.

[43] Safaee A, Sarkar D K, Farzaneh M, "Proceedings of the 2006 NSTI Nanotechnology Conference and Trade Show", Boston, Massachusetts, U.S.A., Vol. 3, pp. 190, May 2006.

[44] Sarkar D K and Farzaneh M, "Proceedings of the 2006 NSTI Nanotechnology Conference and Trade Show", Boston, Massachusetts, USA, Vol. 3, pp. 166, May 2006.

[45] Montero-Moreno J M, Sarret M, Müller C, Surface Coatings Technology 201, 6352, 2007.

[46] Kapaklis V, Georgiopoulos A, Poulopoulos P, Politis C, Physica E 38, 44, 2007.

[47] Garoff N and Zauscher S, Langmuir 18, 6921, 2002.

[48] Mills A, Lee S K, A. Lepre, Parkin I P, O'Neill S A, Photochem. Photobiol. Sci. 1, 865, 2002.

[49] Croutch V K, and Hartley R A, Coat J. Tech., 64, 41, 1991.

[50] Solmo B, and Gupta V, Mech. of mater., 33, 471, 2001.

[51] Anderson D N, and Reich A D, "NASA Technical Memorandum", 107399 AIAAA-97-0303, 1997.

Readers are invited to offer their comments on the article. Please fill in the Reader's Forum.